

Niğde Ömer Halisdemir Üniversitesi Mühendislik Bilimleri Dergisi Niğde Ömer Halisdemir University Journal of Engineering Sciences

Araştırma makalesi / Research article





Identification of fractional order PI controllers ensuring desired gain and phase margins for a time-delayed single-area load frequency control system with demand response

Talep yanıtı ile zaman gecikmeli bir bölgeli yük frekans kontrolü sistemi için istenen kazanç ve faz marjlarını sağlayan kesir dereceli PI denetleyicilerinin tanımlanması

Deniz Katipoğlu 1,* 🗓

¹ Erzurum Technical University, Faculty of Engineering and Architecture, Department of Electrical and Electronics Engineering, Erzurum, Türkiye

Abstract

This research presents a load frequency control (LFC) system with demand response (DR) studied for robust stability analysis based on gain and phase margins (GPMs) utilizing a fractional-order proportional-integral (FOPI) controller. Electric power systems contain many parametric uncertainties. FOPI controller gains are adjustable parameters and can be designed to provide the desired frequency control and dynamic performance. Therefore, in this article, the robust stability regions containing a set of robust FOPI controller gains are designed for the range model of the load frequency control system using Kharitonov's theorem, considering the uncertainties in the LFC-DR system parameters and the time delay. Further, the robust performance of the interval LFC-DR system in terms of design features, including GPMs, is investigated. Simulation studies indicate that GPM parameters provide a better dynamic performance in terms of fast damping of oscillations, less settling time, and overshoot time for the interval LFC-DR system.

Keywords: Gain margin, Phase margin, Demand response, Fractional-order controller, Robust stability region

1 Introduction

A need for renewable energy sources (RESs) has emerged because of the decreasing availability of conventional resources, the environmental effects of greenhouse gas emissions from fossil fuel combustion, and the rapid increase in energy demand [1, 2]. It is challenging to use renewable energy sources for load frequency management because of their drawbacks, such as significant intermittency and power fluctuation [3, 4]. Demand response (DR) is used in load frequency control systems to overcome the intermittency of wind and solar power generation and regulate system frequency and cope with fluctuations in load demand [5-7]. Demand response control is an effective method to shift or reduce the peak load on the demand side (user side) to ensure the balance of production and consumption in the power grid [8]. In the study conducted in

Öz

Bu araştırma, kesir dereceli oransal-integral (KDOI) denetleyici kullanılarak, talep yanıtı (TY) ile yük frekans kontrolü (YFK) sisteminin gürbüzlük analizi için kazanç ve faz marjları (KFM'ler) temelinde incelendiği bir sistemi sunmaktadır. Elektrik güç sistemleri birçok parametre belirsizlik içermektedir. KDOI denetleyici kazançları ayarlanabilir parametrelerdir ve istenen frekans kontrolü ve dinamik performans sağlamak için tasarlanabilirler. Bu nedenle, bu makalede, YFK-TY sistem parametrelerindeki belirsizlikler ve zaman gecikmesi göz bulundurularak, Kharitonov Teoremi kullanılarak yük frekans kontrol sisteminin aralık modelinin tasarımında gürbüz KDOI denetleyici kazançları içeren gürbüzlük bölgeleri tasarlanmıştır. Ayrıca, KFM'ler gibi tasarım özellikleri açısından aralık YFK-TY sisteminin güzbüz performansı incelenmiştir. Simülasyon çalışmaları, KFM parametrelerinin, aralık YFK-TY sistemi için salınımların hızlı bir şekilde sönümlenmesi, yerleşme zamanının ve aşım süresinin daha düşük olması açısından daha iyi bir dinamik performans sağladığını göstermektedir.

Anahtar kelimeler: Kazanç marjı, Faz marjı, Talep yanıtı, Kesir dereceli denetleyici, Sağlamlık bölgesi

[9], frequency control of power systems using renewable energy sources was implemented using demand response and storage battery, utilizing a real 10-bus power system model. In the study conducted in [10], using a simplified model of Australia's eastern seaboard developed in DIgSILENT PowerFactory, it was observed that both DR and large-scale battery energy storage systems (BESSs) effectively reduced frequency deviations. In this way, the reliability and flexibility of load frequency control (LFC) systems are increased. Controlled loads such as air conditioners (ACs), electric water heaters (EWH), HVAC, and thermostatically controlled loads (TCL) are included in frequency control to involve demand response in LFC systems [11-13].

Measurement data and control commands in power systems need to be transmitted back and forth between control centers, stations, and DR, and a private or open

^{*} Sorumlu yazar / Corresponding author, e-posta / e-mail: deniz.katipoglu@erzurum.edu.tr (D. Katipoğlu) Geliş / Received: 02.01.2025 Kabul / Accepted: 14.07.2025 Yayımlanma / Published: 15.10.2025 doi: 10.28948/ngumuh.1612061

communication network that meets the performance needs of the system is needed. When the command signal is being transmitted from the control system to the reacting loads, there are communication delays that could negatively impact the dynamics and stability of the LFC-DR system [14]. Studies have been conducted on calculating the stability time delay margin of time-delayed LFC-DR systems for specific system and controller parameters [15, 16]. However, no studies have been undertaken on obtaining all values of the proportional-integral (PI) controller parameters, known as the stability region, which ensure the stable operation of time-delayed LFC-DR systems.

Because PI controllers are practical, straightforward, and have reliable performance, they are employed to enhance the dynamic behavior of LFC-DR systems [17-19]. In recent years, fractional-order PI (FOPI) controllers have been preferred to improve systems that have experienced parametric uncertainty and external degradation because they provide a greater degree of freedom and flexibility. In this study, a FOPI controller is employed instead of FOPD or FOPID controllers, as the use of these higher-order controllers would increase the dimensionality of the controller space and significantly complicate the stability region analysis. In previous studies [20, 21], researchers used a fractional order PI controller to control a single area timedelayed LFC system. In the study cited [22], a single input interval type-2 fuzzy fractional-order PI (SIT2-FFOPI) controller based on stability boundary locus (SBL) was proposed to be used in the LFC system of the time-delayed microgrid (MG) of a ship. In [23], an efficient and robust FOPID control method called MOGOA-FOPID, using the multi-objective grasshopper optimization (MOGOA) for frequency control in an MG consisting of RESs, diesel generators, FCs, flywheels, and a battery storage system was proposed. A FOPI controller was also used in this study.

This study examines the effect of the FOPI controller of the LFC-DR system that contains parametric uncertainties on robust stability. Kharitonov's Theorem provides a more flexible, faster, and computationally efficient way to determine the stability of systems with parameter uncertainties compared to Lyapunov theory. The Kharitonov method simplifies the analysis and can be applied to timevarying systems as well [24-26]. This study adds to the body of knowledge by using Kharitonov's theorem to evaluate robust stability areas of the interval LFC-DR system that contain communication time delay and a FOPI controller. Firstly, all possible characteristic polynomials of the perturbed interval LFC-DR system are obtained using Kharitonov's theorem. Then, the stability regions in the PI controller plane that will stabilize each Kharitonov polynomial are calculated using a simple graphical method called the stability boundary locus (SBL) method [27, 28]. Lastly, the region that is the intersection of the calculated stability regions, provides the interval system's PI controller plane's robust stability region. This approach has been used to study the stability regions of time-delayed communication systems for large wind turbines [29], time-delayed two-area load-frequency systems based on gain and phase margins

and micro-grid systems [30, 31], and time-delayed one-area load-frequency systems with fractional-order PI controllers and fuel cell micro-grids [20, 32]. One of the principal areas of study in recent years has been the robust stability analysis of fractional-order systems with parametric uncertainty. In the study cited as [33], sixteen Kharitonov polynomials were used for numerator and denominator polynomials of the open loop transfer function of a time-delayed micro-grid system that is time-delayed based on gain and phase margins to design robust FOPI controller gains and robust stability areas were obtained. In the study cited as [34], a robust FOPID controller was designed for LFC systems containing perturbed (interval) non-reheated and reheated turbines using Kharitonov polynomials. In the study cited as [35], an interval fractional order proportional integral derivative (INFOPID) controller was proposed for a two-area LFC system, and Kharitonov polynomials were obtained due to parametric uncertainties. Robust stability areas were found using the stability boundary locus method.

The design of robust PI controllers and the identification of robust stability areas should take into account robust stability margins as well as design elements like gain margins (GM) and phase margins (PM) that guarantee the robust dynamic performance of the interval LFC-DR system. The consideration of GPM in frequency design features such as damping, transcendental, and settling times, which is the second contribution of this study to the literature, also allows us to select several PI controller parameters for frequency responses. A gain-phase margin tester (GPMT) was incorporated into the time-delayed LFC system model in this work as a "virtual compensator" to the forward transfer direction [36, 37].

The following are some of the significant contributions this study made to the literature. A single-area interval LFC-DR system was preferred in the study to demonstrate the effectiveness of the proposed robust controller design at a fundamental level. These contributions focus on gain and phase margin (GPM) based robust stability areas of a time-delayed single-area load frequency control (LFC) system that includes demand response (DR) and fractional order proportional integral (FOPI) controller:

- The robust stability areas of the interval LFC-DR system with a FOPI controller were determined under parametric uncertainties using the Kharitonov theorem and the SBL approach.
- After studying how the fractional value affected the integral controller's robust stability areas, it was found that utilizing a FOPI controller expanded those regions.
- A load change scenario was created, and through timedomain simulations, the robust stability areas' performances were examined [38].
- Finally, using FOPI controllers chosen from the regions, the performance of the system was evaluated along with the impact of GPMs on robust stability areas. GPMs have been seen to enhance the system's performance.

This article consists of five parts. A model of a timedelayed single-area interval LFC-DR system with a GPMTattached FOPI controller is shown in Section 2. In Section 3, the application of the Kharitonov theorem and the SBL method for calculating the robust stability areas is presented in detail. In Section 4, the proposed method is applied to a single-area interval LFC-DR control system, the robust stability areas based on the FOPI controller and GPMs are calculated, and the results of time domain simulations are presented. The conclusion of the article is presented in Section 5.

Model of single area a time-delayed LFC-DR system

Power systems are large-scale systems represented by nonlinear dynamics. Figure 1 shows the model of a single area interval LFC-DR system with a time delay and added GPMT and, the FOPI controller is used as load frequency controller. Furthermore, on the DR side, a proportionalintegral type controller (PI) is used [15]. The model of interval LFC-DR consists of a load, a generator and governor, a thermal turbine, and droop characteristics. The system model's parameter nomenclature is given. With the addition of the DR to the LFC system, the required control effort is denoted by Ω , showing the sharing between the DR and conventional generation units [39]:

$$\Delta P_g(s) = \alpha_0 \Omega$$

$$\Delta P_{DR}(s) = \alpha_1 \Omega$$
(1)

The sharing factor of the conventional turbine-generator system is α_0 and the DR control loop is α_1 , and their sum is equal to one. Also, λ , K_I , and K_P refer to the fractional-order value of the integral controller and the FOPI controller gain values. To perform various control functions in the system, it is necessary to consider the measurement and communication time delays between the classical production unit and the central controller. The total amount of communication delay is τ , represented by the expression $e^{-s\tau}$ in the LFC system.

$$G(s) = \frac{\Delta f}{\Delta X_C} = \frac{G_T(s)G_G(s)G_L(s)}{1 + G_{DR}(s)G_L(s) + G_T(s)G_G(s)G_L(s)/R}$$
(2)

where

• The governor dynamics are as follows:

$$G_G(s) = \frac{\Delta X_g}{\Delta X_c} = \frac{1}{1 + sT_g} \tag{3}$$

• The turbine dynamics are as follows:
$$G_T(s) = \frac{\Delta P_g}{\Delta X_g} = \frac{1 + sF_pT_r}{(1 + sT_r)(1 + sT_c)} \tag{4}$$

• The power system (load and generator) dynamics are as follows:

$$G_L(s) = \frac{\Delta f}{\Delta P_L} = \frac{1}{D + sM} \tag{5}$$

• The demand response dynamics are as follows:

$$G_{DR}(s) = \frac{\Delta f}{\Delta P_{DR}} = K_{P(DR)} + \frac{K_{I(DR)}}{s}$$
 (6)

• $G_C(s)$ is FOPI controller as follows:

$$G_C(s) = K_P + \frac{K_I}{s^{\lambda}} \tag{7}$$

where λ is the fractional order of the integral controller and its value is chosen from $0 \le \lambda \le 2$ [40]. To calculate the robust stability regions and apply Kharitonov's theorem to the timedelayed interval LFC-DR system with a FOPI controller, the transfer function of the interval LFC-DR system can be represented as follows using Equations (3)-(6):

$$G(s) = \frac{N(s)}{D(s)} = \frac{b_2 s^2 + b_1 s}{a_5 s^5 + a_4 s^4 + a_3 s^3 + a_2 s^2 + a_1 s + a_0}$$
(8)

where the coefficients of N(s) and D(s) polynomials, $a_i(i =$ 0,1,2,3,4,5) and $b_i(i = 1,2)$, are given as Equation (26) in Appendix A in terms of interval LFC-DR system parameters.

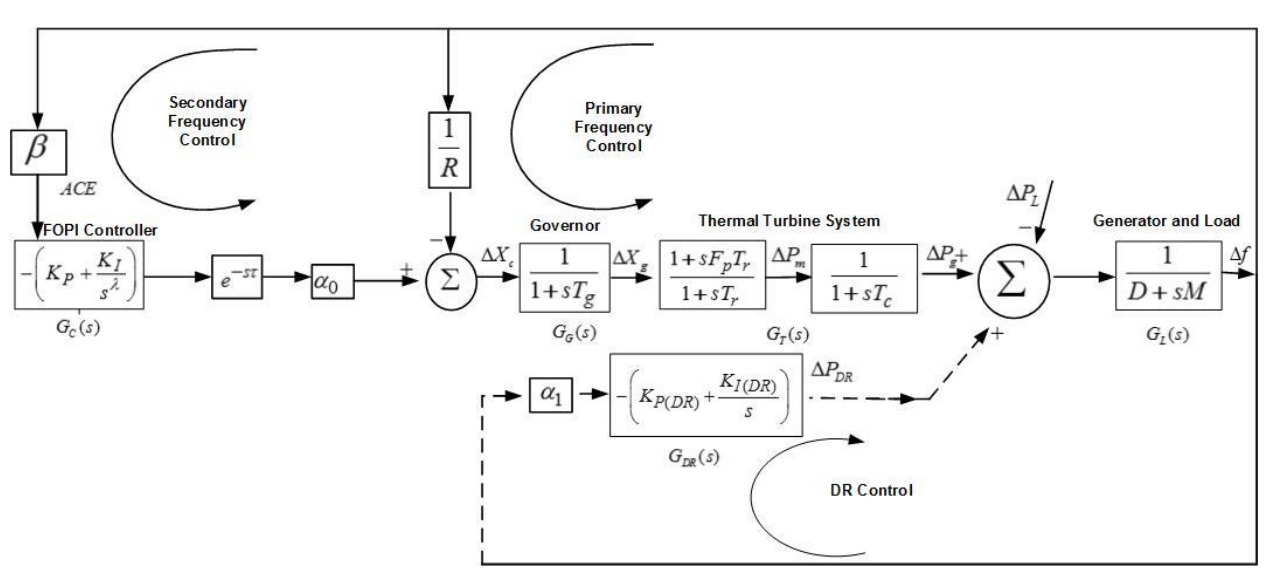


Figure 1. Block diagram of LFC-DR system with an additional GPMT and FOPI controller

3 Calculation of the robust stability regions

3.1 Kharitonov's theorem

In control systems, uncertainties in system parameters, changes in load, and errors in modeling the system could reduce system performance and cause system instability. Kharitonov's theorem is a graphical technique used to examine the interval polynomials' stability, whose complex or real coefficients vary within a certain interval [41, 42]. According to this theorem, four vertex polynomials are obtained by utilizing the maximum and minimum values of the given coefficient range from an interval polynomial whose coefficients vary within a certain range. The polynomials are considered stable if all four of them are Routh Hurwitz stable. Kharitonov polynomials are as shown in Equation (9) and (10).

$$N_{1}(s) = \underline{b_{1}}s + \overline{b_{2}}s^{2}$$

$$N_{2}(s) = \overline{b_{1}}s + \overline{b_{2}}s^{2}$$

$$N_{3}(s) = \underline{b_{1}}s + \underline{b_{2}}s^{2}$$

$$N_{4}(s) = \overline{b_{1}}s + b_{2}s^{2}$$

$$(9)$$

$$D_{1}(s) = \underline{\alpha_{0}} + \underline{\alpha_{1}}s + \overline{\alpha_{2}}s^{2} + \overline{\alpha_{3}}s^{3} + \underline{\alpha_{4}}s^{4} + \underline{\alpha_{5}}s^{5}$$

$$D_{2}(s) = \underline{\alpha_{0}} + \overline{\alpha_{1}}s + \overline{\alpha_{2}}s^{2} + \underline{\alpha_{3}}s^{3} + \underline{\alpha_{4}}s^{4} + \overline{\alpha_{5}}s^{5}$$

$$D_{3}(s) = \overline{\alpha_{0}} + \underline{\alpha_{1}}s + \underline{\alpha_{2}}s^{2} + \overline{\alpha_{3}}s^{3} + \overline{\alpha_{4}}s^{4} + \underline{\alpha_{5}}s^{5}$$

$$D_{4}(s) = \overline{\alpha_{0}} + \overline{\alpha_{1}}s + \underline{\alpha_{2}}s^{2} + \underline{\alpha_{3}}s^{3} + \overline{\alpha_{4}}s^{4} + \overline{\alpha_{5}}s^{5}$$

$$(10)$$

where $N_k(s)$ and $D_l(s)$ (k, l=1,2,3,4) are vertex polynomials of G(s) given in Equation (8). The coefficient of vertex polynomials $\underline{\alpha_i} \leq \underline{\alpha_i} \leq \overline{\alpha_i}$ $(\underline{\alpha_i}, \overline{\alpha_i} \neq 0, i=0,1,2,3,4,5)$ and $\underline{b_i} \leq b_i \leq \overline{b_i}$ $(\underline{b_i}, \overline{b_i} \neq 0, i=1,2)$ represent the minimum and maximum value of perturbed system parameters of the interval LFC-DR system. The values of the interval coefficients given by Equations (9) and (10) are given as Equation (27) in Appendix A. Using Equations (9) and (10), the set of sixteen transfer functions for the interval model of the LFC-DR system including FOPI given in Equation (8) can be formed as,

$$G_i(s) = \frac{N_k(s)}{D_l(s)}$$

$$i = 1,2,3,...,16, \qquad k = 1,2,3,4, \qquad l = 1,2,3,4.$$
(11)

3.2 Identification of fractional order PI controller for interval LFC-DR system

This section suggests a procedure for designing the FOPI controller in the time-delayed single-area interval LFC-DR system using a GPMT. In this technique, the GPMT $C(A, \phi) = Ae^{-j\phi}$ is introduced to the feed-forward loop of the interval LFC-DR system as shown in Figure 1. Here, A and ϕ represent gain margin and phase margin. The GPMT does not exist in the physical system; it is merely a virtual compensator to specify the desired frequency parameters.

The system's overall closed-loop transfer function is as follows:

$$\frac{G(s)C(Ae^{-j\phi})G_C(s)\beta\alpha_0e^{-s\tau}}{1+G(s)C(Ae^{-j\phi})G_C(s)\beta\alpha_0e^{-s\tau}}$$
(12)

The following form should be used to indicate the entire system's characteristics equation:

$$\Delta(s,\lambda,\tau) = P(s,\lambda) + Q(s,\lambda)e^{-(s\tau+j\phi)}$$
 (13)

$$P(s,\lambda) = p_5 s^{5+\lambda} + p_4 s^{4+\lambda} + p_3 s^{3+\lambda} + p_2 s^{2+\lambda} + p_1 s^{1+\lambda} + p_0 s^{\lambda}$$

$$Q(s,\lambda) = q_3 s^{\lambda+2} + q_2 s^{\lambda+1} + q_1 s^2 + q_0 s$$
(14)

where p and q coefficients depending on the parameters of the interval LFC-DR system are given as Equation (28) in the Appendix A. To identify the stability regions, first substitute $s=j\omega$ with $\omega>0$ in Equation (14), we get,

$$\Delta(j\omega, \lambda, \tau) = p_{5}(j\omega)^{5+\lambda} + p_{4}(j\omega)^{4+\lambda} + p_{3}(j\omega)^{3+\lambda} + p_{2}(j\omega)^{2+\lambda} + p_{1}(j\omega)^{1+\lambda} + p_{0}(j\omega)^{\lambda} + K_{P}(q'_{3}(j\omega)^{2+\lambda} + q'_{2}(j\omega)^{1+\lambda})e^{-j(\omega\tau+\phi)} + K_{I}(q''_{1}(j\omega)^{2} + q''_{0}(j\omega))e^{-j(\omega\tau+\phi)} = 0$$
(15)

It is to be noted that q' and q'' coefficients in Equation (15) do not contain K_P and K_I . These coefficients are given as Equation (28) in the Appendix A depending on the interval LFC-DR system parameters. Solving Equation (15) using the mathematical identities,

$$e^{-j(\omega\tau+\phi)} = \cos(\omega\tau+\phi) - j\sin(\omega\tau+\phi)$$
$$j^{\lambda} = \cos(\frac{\lambda\pi}{2}) + j\sin(\frac{\lambda\pi}{2})$$
 (16)

Substituting Equation (16) into Equation (15), we can obtain the equation separating the imaginary and real parts as:

$$\begin{split} p_5\omega^{5+\lambda} \left\{ \cos(5+\lambda) \frac{\pi}{2} + j \sin(5+\lambda) \frac{\pi}{2} \right\} + \\ p_4\omega^{4+\lambda} \left\{ \cos(4+\lambda) \frac{\pi}{2} + j \sin(4+\lambda) \frac{\pi}{2} \right\} + \\ p_3\omega^{3+\lambda} \left\{ \cos(3+\lambda) \frac{\pi}{2} + j \sin(3+\lambda) \frac{\pi}{2} \right\} + \\ p_2\omega^{2+\lambda} \left\{ \cos(2+\lambda) \frac{\pi}{2} + j \sin(2+\lambda) \frac{\pi}{2} \right\} + \\ p_1\omega^{1+\lambda} \left\{ \cos(1+\lambda) \frac{\pi}{2} + j \sin(1+\lambda) \frac{\pi}{2} \right\} + \\ p_0\omega^{\lambda} \left\{ \cos \frac{\lambda\pi}{2} + j \sin \frac{\lambda\pi}{2} \right\} + \\ \cos(\omega\tau + \phi) - \end{split}$$

$$j\sin(\omega\tau + \phi) \begin{cases} K_{P}(q_{3}'\omega^{2+\lambda}) \left\{ \cos(2+\lambda)\frac{\pi}{2} + \atop j\sin(2+\lambda)\frac{\pi}{2} \right\} + \\ q_{2}'\omega^{1+\lambda} \left\{ \cos(1+\lambda)\frac{\pi}{2} + \atop j\sin(1+\lambda)\frac{\pi}{2} \right\} + \\ K_{I}(-q_{1}''\omega^{2} + jq_{0}''\omega) \\ = 0 \end{cases}$$

$$(17)$$

$$\Delta(j\omega,\lambda,\tau) = \Re(\Delta(j\omega,\lambda,\tau)) + j\Im(\Delta(j\omega,\lambda,\tau)) = 0 \Delta(j\omega,\lambda,\tau) = K_P A_1(\omega) + K_I B_1(\omega) + C_1(\omega) + j[K_P A_2(\omega) + K_I B_2(\omega) + C_2(\omega)] = 0 \text{where } A_i, B_i, \text{ and } C_i \ (i = 1,2) \text{ polynomials expressions are:}$$

$$A_{1}(\omega) = q_{3}'\omega^{2+\lambda}(\cos(\omega\tau + \phi)(\cos(2+\lambda)\frac{\pi}{2}) + \sin(\omega\tau + \phi)(\sin(2+\lambda)\frac{\pi}{2})) + q_{2}'\omega^{2+\lambda}(\cos(\omega\tau + \phi)(\cos(2+\lambda)\frac{\pi}{2}) + \sin(\omega\tau + \phi)(\sin(2+\lambda)\frac{\pi}{2}));$$

$$B_{1}(\omega) = -q_{1}''\omega^{2}\cos(\omega\tau + \phi) + q_{0}''\omega\sin(\omega\tau + \phi);$$

$$C_{1}(\omega) = p_{5}\omega^{5+\lambda}\cos(5+\lambda)\frac{\pi}{2} + p_{4}\omega^{4+\lambda}\cos(4+\lambda)\frac{\pi}{2} + p_{3}\omega^{3+\lambda}\cos(3+\lambda)\frac{\pi}{2} + p_{2}\omega^{2+\lambda}\cos(2+\lambda)\frac{\pi}{2} + p_{1}\omega^{1+\lambda}\cos(1+\lambda)\frac{\pi}{2} + p_{0}\omega^{\lambda}\cos\frac{\lambda\pi}{2};$$

$$A_{2}(\omega) = q_{3}'\omega^{2+\lambda}(-\sin(\omega\tau + \phi)(\cos(2+\lambda)\frac{\pi}{2}) + \cos(\omega\tau + \phi)(\sin(2+\lambda)\frac{\pi}{2}) + cos(\omega\tau + \phi)(\sin(2+\lambda)\frac{\pi}{2}) + \cos(\omega\tau + \phi)(\sin(2+\lambda)\frac{\pi}{2});$$

$$B_{2}(\omega) = q_{1}''\omega^{2}\sin(\omega\tau + \phi) + q_{0}''\omega\cos(\omega\tau + \phi);$$

$$C_{2}(\omega) = p_{5}\omega^{5+\lambda}\sin(5+\lambda)\frac{\pi}{2} + p_{4}\omega^{4+\lambda}\sin(4+\lambda)\frac{\pi}{2} + p_{3}\omega^{3+\lambda}\sin(3+\lambda)\frac{\pi}{2} + p_{4}\omega^{4+\lambda}\sin(4+\lambda)\frac{\pi}{2} + p_{3}\omega^{3+\lambda}\sin(3+\lambda)\frac{\pi}{2} + p_{2}\omega^{2+\lambda}\sin(2+\lambda)\frac{\pi}{2} + p_{1}\omega^{1+\lambda}\sin(1+\lambda)\frac{\pi}{2} + p_{2}\omega^{2+\lambda}\sin(2+\lambda)\frac{\pi}{2} + p_{1}\omega^{1+\lambda}\sin(1+\lambda)\frac{\pi}{2}$$

$$p_{0}\omega^{\lambda}\sin\frac{\lambda\pi}{2}$$

Setting both the imaginary and real parts equating to 0, we obtain:

$$K_P A_1(\omega) + K_I B_1(\omega) + C_1(\omega) = 0$$

 $K_P A_2(\omega) + K_I B_2(\omega) + C_2(\omega) = 0$ (20)

Depending on ω crossing frequency, Equation (20) solved for (K_P, K_I) to achieve the stability boundary locus $\ell(K_P, K_I, \omega)$ in the (K_P, K_I) plane shown as:

$$K_{P} = \frac{B_{1}(\omega)C_{2}(\omega) - B_{2}(\omega)C_{1}(\omega)}{A_{1}(\omega)B_{2}(\omega) - A_{2}(\omega)B_{1}(\omega)}$$

$$K_{I} = \frac{A_{2}(\omega)C_{1}(\omega) - A_{1}(\omega)C_{2}(\omega)}{A_{1}(\omega)B_{2}(\omega) - A_{2}(\omega)B_{1}(\omega)}$$
(21)

For a fixed τ and λ , the solution to these two equations in Equation (21) is referred to as the interval LFC-DR system's complex root boundaries (CRBs). In addition to these stability boundaries, for $\omega=0$ from Equation (20) such a stability change occurs only for $K_I = 0$ and is called the real root boundary (RRB) of the stability region. Consequently, the RRB and CRB locus divide the (K_P, K_I) -plane into stable and unstable regions. The PI controller values to stabilize each Kharitonov polynomial are calculated by following the steps shown in Equations (13)-(21). Sixteen stability regions are calculated in the PI controller parameter space defined as $\Delta_n(s, \lambda, \tau)$ with each Kharitonov polynomial n=1,2,...,16. The intersection of these sixteen stability areas, which is described as follows, indicates a region with robust PI controller gains that ensure the interval LFC-DR system remains stable despite uncertainties in the interval LFC-DR system parameters:

$$\ell_I(K_P, K_I, \omega) = \bigcap_{n=1}^{16}, \ell_n(K_P, K_I, \omega)$$
 (22)

4 Results

This section presents the robust stability region results for the time-delayed single-area interval LFC-DR system with FOPI and GPM specifications. The Kharitonov theorem is primarily applicable to interval polynomial systems and cannot be directly applied to time-delay or non-polynomial systems. Similarly, the SBL method may become computationally intensive for high-order systems and, due to the discrete nature of frequency sweeping, may only provide approximate stability boundaries. Following this analysis, verification studies are carried out under large disturbance events involving load fluctuations. The parameters of the interval LFC-DR system are provided in Table 1.

Table 1. LFC-DR system parameters [43]

Parameters	M	D	F_P	R	β	T_g	T_c	T_r
	8.8	1	1/6	1/11	21	0.2	0.3	12

The steps of applying the Kharitonov theorem to the interval LFC-DR system are given as follows:

Step 1: In the interval LFC-DR system, $\delta=\pm 10\%$ parametric uncertainty is assumed the time delay value is $\tau=Is$ and the controller parameters DR participation $K_{P(DR)}=0.5$ and $K_{I(DR)}=0.7$ are selected based on their frequent use in the literature as reference parameters for analyzing system performance under various conditions [44, 45]. In addition, the participation factors of the classical production unit and DR group are determined as $\alpha_0=0.6$ and $\alpha_1=0.4$ [15], the fractional order degree is $\lambda=0.8$, and it is assumed that the system is without GPM specifications

 $(A = 1, \phi = 0^{\circ})$. The minimum and maximum values of the system parameters are calculated as follows:

$$\begin{split} M \in [7.92; 9.68], D \in [0.9; 1.1], \\ F_P \in [0.15; 0.1833], R \in [0.0818; 0.1], \\ T_a \in [0.18; 0.22], T_c \in [0.27; 0.33], T_r \in [10.8; 13.2] \end{split}$$

Step 2: The upper and lower limit values of the transfer function G(s) and coefficients are obtained as follows:

$$G(s) = \frac{\left[\underline{b_2} \quad \overline{b_2}\right] s^2 + \left[\underline{b_1} \quad \overline{b_1}\right] s}{\left[\underline{a_5} \quad \overline{a_5}\right] s^5 + \left[\underline{a_4} \quad \overline{a_4}\right] s^4 + \left[\underline{a_3} \quad \overline{a_3}\right] s^3 + \left[\underline{a_2} \quad \overline{a_2}\right] s^2 + \left[\underline{a_1} \quad \overline{a_1}\right] s + \left[\underline{a_0} \quad \overline{a_0}\right]}$$

$$a_0 \in \left[\underline{a_0} \quad \overline{a_0}\right] = [0.0229 \quad 0.028];$$

$$a_1 \in \left[\underline{a_1} \quad \overline{a_1}\right] = [1.3477 \quad 1.515];$$

$$a_2 \in \left[\underline{a_2} \quad \overline{a_2}\right] = [3.3930 \quad 5.3808];$$

$$a_3 \in \left[\underline{a_3} \quad \overline{a_3}\right] = [7.7438 \quad 14.2901];$$

$$a_4 \in \left[\underline{a_4} \quad \overline{a_4}\right] = [3.2280 \quad 7.2225];$$

$$a_5 \in \left[\underline{a_5} \quad \overline{a_5}\right] = [0.3401 \quad 0.9277];$$

$$b_1 \in \left[\underline{b_1} \quad \overline{b_1}\right] = [1.0309 \quad 1.26];$$

$$b_2 \in \left[\underline{b_2} \quad \overline{b_2}\right] = [1.6701 \quad 3.0492].$$
(24)

Step 3: Sixteen characteristic equations are obtained by substituting in Equation (13) the lower and upper limit values of the characteristic equation coefficients found in Step 2. Then, with the help of the SBL method given in Equations (16) - (21), the stability region for each vertex polynomial of the system is obtained. Finally, the robust stability region represented by the shaded area in Figure 2 is produced by the intersection of the sixteen stability areas obtained using vertex polynomials.

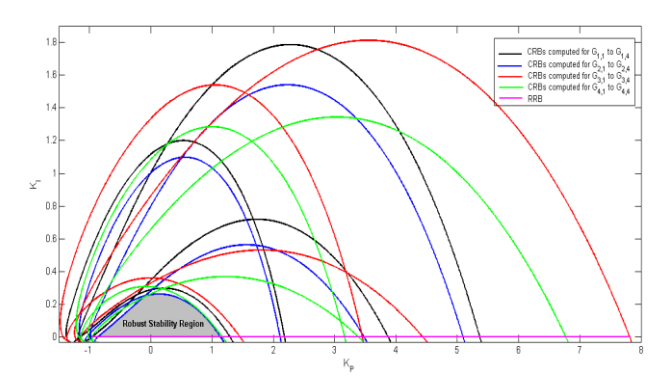


Figure 2. The stability regions and robust stability region obtained from vertex polynomials for $\lambda = 0.8$ and $\tau = 1s$

Moreover, to investigate the impact of fractional-order parameters on the robust stability regions four different fractional-order parameters are selected, i.e., $\lambda=0.6$, $\lambda=0.8$, $\lambda=1$ and $\lambda=1.2$, whereas A=1, $\phi=0^{\circ}$, the time delay is fixed at $\tau=1s$, participation factors $\alpha_0=0.6$ and $\alpha_1=0.4$, uncertainty of $\delta=\pm10\%$. As may be seen in Figure 3 the size

of robust stability regions increases when the fractionalorder parameter value is smaller than one ($\lambda < I$) and the size of robust stability regions decreases when the fractionalorder parameter value is bigger than one $(\lambda \ge I)$. To examine the interval LFC-DR system's frequency response, a load change scenario graph is created and applied to the system as shown in Figure 4. The system's frequency response under the effect of load disturbance is shown in Figure 5 at the robust PI parameter ($K_P = 0.5, K_I = 0.13$) indicated with '*' selected over the robust stability regions obtained by using different fraction order values from Figure 3. Table 2 illustrates how the system performs better when the frequency response $\lambda < 1$, and a significant decrease in peak overshoots of frequency deviation. In addition, for all fractional-order values, it is seen that the oscillations in the frequency response of the system are damped in a short time and the system reaches stability.

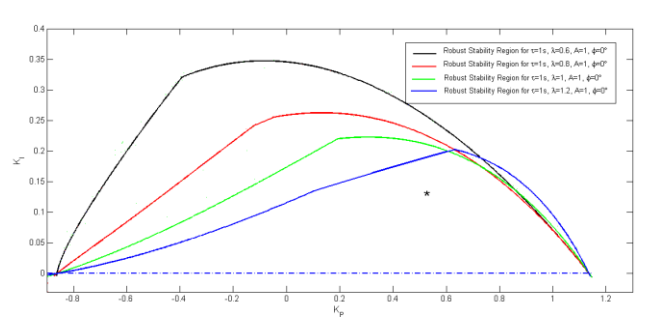


Figure 3. Robust stability regions for different fractional order values

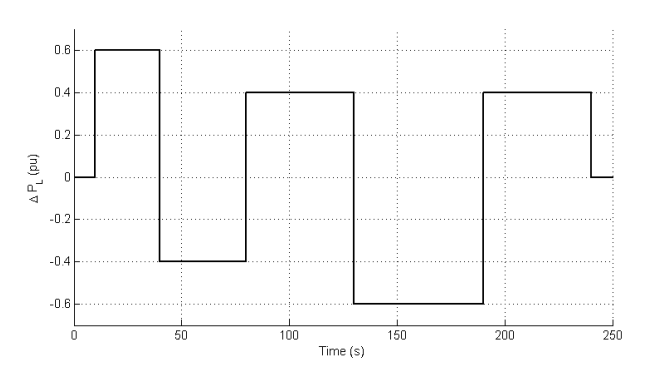


Figure 4. Load variation graph applied to the interval LFC-DR system

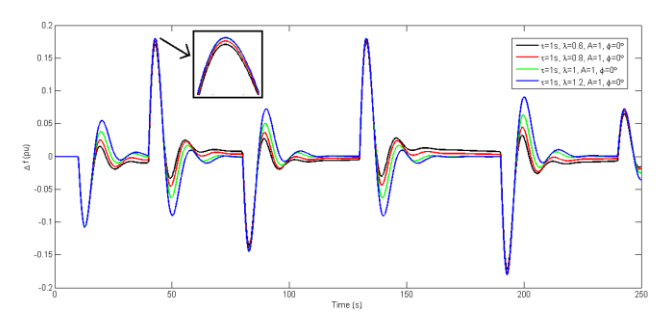


Figure 5. Different fractional order values on the system's frequency response

Table 2. Frequency response performance metrics for different λ values

λ value	Rise Time (s)	Settling Time (s)	Overshoot (Hz)
0.6	5.0	65	0.1742
0.8	5.5	67	0.1772
1.0	6.2	69	0.1798
1.2	7.0	72	0.1803

Also, the change of the robust stability regions for parametric uncertainties of $\delta=\pm0\%$, $\delta=\pm5\%$, $\pm8\%$, $\pm11\%$, and $\pm 14\%$ are obtained. For this case, the time delay, fractionalorder value, and GPM specifications are chosen as $\tau=2s$, $\lambda = 0.8$ and A = 1, $\phi = 0^{\circ}$ and the robust stability regions are displayed in Figure 6. As seen in Figure 6, as the rate of change in the system parameters, that is, the uncertainty in the interval LFC-DR system parameters, increases, the robust stability regions become smaller. Moreover, the effects of gain and/or phase margins on the robust stability regions are investigated and the time delay, variations in system parameters, fractional order degree, and the crossing frequency range are selected as $\tau=1s$, $\delta=\pm10\%$, $\lambda=0.8$ and $\omega \in [0, 1.1]$, respectively. Firstly, a specific PM is chosen as $\phi = 20^{\circ} (A=I)$ and the robust stability region is calculated using Equations (15)-(22) and shown in Figure 7. Similarly, Kharitonov theorem Equations (15)-(22) is employed to identify the robust stability region for specific GM as A=1.5 $(\phi = 0^{\circ})$ and is depicted in Figure 7. As can be seen from Figure 7 the robust stability region for $\phi = 20^{\circ} (A=I)$ is much smaller as compared with the robust region for A =1.5 ($\phi = 0^{\circ}$). It is seen that the gain margin is more effective on the robust stability regions than the phase margin. Finally, using Equations (15)–(22), the robust stability region not having GPM specification ($A = 1, \phi = 0^{\circ}$) is calculated and displayed in Figure 7. When compared to specific PM and GM, the robust regions without GPM specification are significantly larger. Finally, the PI controller gains selected from the robust stability regions shown with '*' in Figure 7 and the test scenario in Figure 4 are applied to the interval LFC-DR system and the frequency responses are examined within t=250s. These PI controller gains are $(K_P = 0.3, K_I =$ 0.05) in $\phi = 20^{\circ} (A = 1)$, $K_P = 0.1944$, $K_I = 0.1226$) in $A = 1.5 \ (\phi = 0^{\circ})$ and $(K_P = 0.0927, K_I = 0.2401)$ in A = $1, \phi = 0^{\circ}$, respectively. The robust frequency responses of the interval LFC-DR in this case are shown in Figure 8 for three robust controller parameters. As illustrated in Figure 8, it is seen that for all three robust PI controller parameters, the oscillations in the frequency response of the system are damped in a short time and the system reaches stability. Preliminary analyses revealed that altering either K_P or K_I while holding the other constant results in comparable dynamics and performance characteristics. Consequently, consistent with established practices in the literature and to facilitate a clearer comparative evaluation, K_P was fixed while K_I is systematically varied throughout the study [46]. Additionally, Table 3 shows that the system's performance characteristics, such as settling time, overshoot, and rising time, are improved by gain and/or phase margin

specifications as compared to the dynamical response in the absence of GPMs ($A = 1, \phi = 0^{\circ}$).

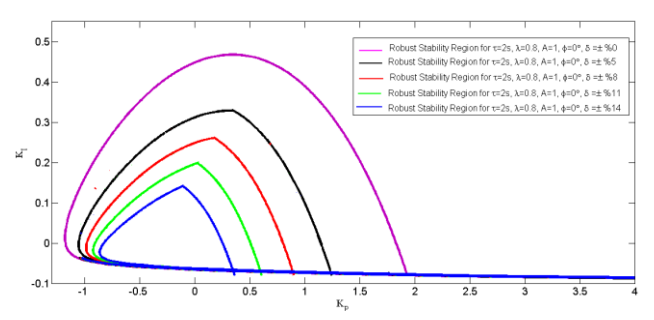


Figure 6. Robust stability regions at different rates of change of system parameters

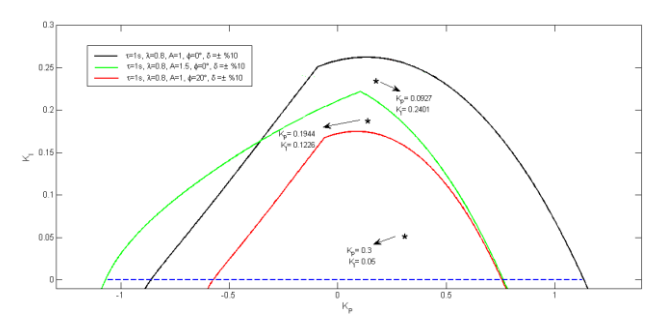


Figure 7. Robust stability regions for GPMs

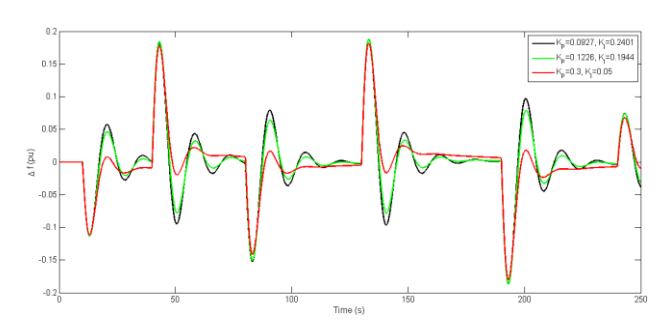


Figure 8. Frequency responses for robust PI parameters selected from robust stability regions

Table 3. Frequency response performance metrics for different control parameter values

Parameter Values	Rise Time (s)	Settling Time (s)	Overshoot (Hz)
Kp=0.0927, Ki=0.2401	3.8	22	0.18
Kp=0.1226, Ki=0.1944	4.2	25	0.19
Kp=0.3, Ki=0.05	5.5	15	0.17

5 Conclusion

In conclusion, using Kharitonov's theorem, this study has demonstrated the impact of GPMs and the fractional order PI controller on robust stability regions of the time-delayed interval LFC-DR system. Using this technique, the robust PI values are calculated, which ensures the robust stability and

performance of the interval LFC-DR system. The findings indicate that when λ is smaller than 1, robust stability regions widen, enhancing the system's robustness margin compared to the PI controller. Additionally, it has been noted that the robust PI values chosen from the robust stability regions based on GPMs exhibit better dynamic performance, as seen by reduced settling times and fast damping. Lastly, the impact of the uncertainty ratio on the system parameters on the robust stability regions is investigated and it is found that the robust stability regions shrink with increasing uncertainty. Future work will focus on the computation of stability regions of multi-area LFC-DR systems with FOPI controllers including incommensurate time delays.

Appendix A

Coefficients of N(s) and D(s) expressed in Equation (8) are as follows:

$$a_{5} = MRT_{g}T_{c}T_{r}; a_{4} = MRT_{r}(T_{g} + T_{c}) + MRT_{g}T_{c} + DRT_{g}T_{r}T_{c} + \alpha_{1}RK_{P(DR)}T_{g}T_{r}T_{c};$$

$$a_{3} = MR(T_{g} + T_{c}) + MRT_{r} + DRT_{r}(T_{g} + T_{c}) + DRT_{g}T_{c} + \alpha_{1}RK_{P(DR)}T_{r}(T_{g} + T_{c}) + \alpha_{1}RK_{P(DR)}T_{g}T_{c} + \alpha_{1}RK_{I(DR)}T_{g}T_{r}T_{c},$$

$$a_{2} = MR + DRT_{r} + DR(T_{g} + T_{c}) + \alpha_{1}RK_{P(DR)}(T_{g} + T_{c}) + \alpha_{1}RK_{I(DR)}T_{g}T_{c} + \alpha_{1}RK_{I(DR)}T_{r}(T_{g} + T_{c}) + F_{p}T_{r} + \alpha_{1}RK_{P(DR)}T_{r};$$

$$a_{1} = 1 + DR + \alpha_{1}RK_{P(DR)} + \alpha_{1}RK_{I(DR)}T_{r} + \alpha_{1}RK_{I(DR)}(T_{g} + T_{c}); a_{0} = \alpha_{1}RK_{I(DR)};$$

$$b_{2} = RF_{p}T_{r}; b_{1} = R.$$
(26)

The minimum and maximum value of G(s) in Equation (9) and (10) are:

$$\begin{split} a_5 &= \underline{M} \underline{R} \underline{T}_g \underline{T}_c \underline{T}_r; \overline{a}_5 = \overline{M} \overline{R} \overline{T}_g \overline{T}_c \overline{T}_r; \\ a_4 &= \underline{M} \underline{R} \underline{T}_r (T_g + T_c) + \underline{M} \underline{R} \underline{T}_g \underline{T}_c + \\ \underline{D} \underline{R} \underline{T}_g \underline{T}_r \underline{T}_c + \alpha_1 \underline{R} K_{P(DR)} \underline{T}_g \underline{T}_r \underline{T}_c; \\ \overline{a}_4 &= \overline{M} \overline{R} \overline{T}_r (\overline{T}_g + \overline{T}_c) + \overline{M} \overline{R} \overline{T}_g \overline{T}_c \\ \overline{D} \overline{R} \overline{T}_g \overline{T}_r \overline{T}_c + \alpha_1 \overline{R} K_{P(DR)} \overline{T}_g \overline{T}_r \overline{T}_c; \\ a_3 &= \underline{M} \underline{R} (T_g + T_c) + \underline{M} \underline{R} \underline{T}_r \\ + \underline{D} \underline{R} \underline{T}_r (T_g + T_c) + \underline{D} \underline{R} \underline{T}_g \underline{T}_c + \\ \alpha_1 \underline{R} K_{P(DR)} \underline{T}_r (T_g + T_c) + \alpha_1 \underline{R} K_{P(DR)} \underline{T}_g \underline{T}_c + \\ \alpha_1 \underline{R} K_{I(DR)} \underline{T}_g \underline{T}_r \underline{T}_c; \overline{a}_3 &= \overline{M} \overline{R} (\overline{T}_g + \overline{T}_c) + \\ \overline{D} \overline{R} \overline{T}_r (\overline{T}_g + \overline{T}_c) + \overline{D} \overline{R} \overline{T}_g \overline{T}_c + \\ \alpha_1 \overline{R} K_{P(DR)} \overline{T}_r (\overline{T}_g + \overline{T}_c) + \alpha_1 \overline{R} K_{P(DR)} \overline{T}_g \overline{T}_c \\ + \alpha_1 \overline{R} K_{I(DR)} \overline{T}_g \overline{T}_r \overline{T}_c; a_2 &= \underline{M} \underline{R} + \underline{D} \underline{R} \underline{T}_r \\ + \underline{D} \underline{R} (T_g + T_c) + \alpha_1 \underline{R} K_{P(DR)} (T_g + T_c) + \\ \end{split}$$

$$\alpha_{1}RK_{I(DR)}T_{g}T_{c} + \alpha_{1}RK_{I(DR)}T_{r}(T_{g} + T_{c}) +$$

$$F_{p}T_{r} + \alpha_{1}RK_{P(DR)}T_{r}; \overline{\alpha_{2}} = \overline{M}\overline{R} + \overline{D}\overline{R}\overline{T_{r}} +$$

$$\overline{D}\overline{R}(\overline{T_{g}} + \overline{T_{c}}) + \alpha_{1}\overline{R}K_{P(DR)}(\overline{T_{g}} + \overline{T_{c}}) +$$

$$+\alpha_{1}\overline{R}K_{I(DR)}\overline{T_{g}}\overline{T_{c}} + \alpha_{1}\overline{R}K_{I(DR)}\overline{T_{r}}(\overline{T_{g}} + \overline{T_{c}}) +$$

$$\overline{F_{p}}\overline{T_{r}} + \alpha_{1}\overline{R}K_{P(DR)}\overline{T_{r}}; a_{1} = 1 + D\underline{R} + \alpha_{1}RK_{P(DR)} +$$

$$+\alpha_{1}RK_{I(DR)}T_{r} + \alpha_{1}RK_{I(DR)}(T_{g} + T_{c});$$

$$\overline{\alpha_{1}} = 1 + \overline{D}\overline{R} + \alpha_{1}\overline{R}K_{P(DR)} + \alpha_{1}\overline{R}K_{I(DR)}\overline{T_{r}} +$$

$$\alpha_{1}\overline{R}K_{I(DR)}(\overline{T_{g}} + \overline{T_{c}}); a_{0} = \alpha_{1}RK_{I(DR)};$$

$$\overline{\alpha_{0}} = \alpha_{1}\overline{R}K_{I(DR)}; b_{2} = RF_{p}T_{r}; \overline{b_{2}} = \overline{R}F_{p}\overline{T_{r}};$$

$$b_{1} = R; \overline{b_{1}} = \overline{R}$$

Coefficients of $P(s,\lambda)$ and $Q(s,\lambda)$ expressed in Equation (14) are as follows:

$$p_{5} = a_{5}; p_{4} = a_{4}; p_{3} = a_{3}; p_{2} = a_{2}; p_{1} = a_{1};$$

$$p_{0} = a_{0};$$

$$q_{3} = A\alpha_{0}\beta K_{P}b_{2}; q_{2} = A\alpha_{0}\beta K_{P}b_{1};$$

$$q_{1} = A\alpha_{0}\beta K_{I}b_{2}; q_{0} = A\alpha_{0}\beta K_{I}b_{1}$$

$$q'_{3} = A\alpha_{0}\beta b_{2}; q'_{2} = A\alpha_{0}\beta b_{1}; q''_{1} = A\alpha_{0}\beta b_{2};$$

$$q''_{0} = A\alpha_{0}\beta b_{1}.$$
(28)

Conflict of Interest

The authors declare that there is no conflict of interest.

Similarity rate (iThenticate): 19%

References

- [1] C. Ghenai, T. Salameh, A. Merabet, Technico-economic analysis of off grid solar PV/Fuel cell energy system for residential community in desert region. International Journal of Hydrogen Energy, 45(20),11460-11470, 2020. https://doi.org/10.1016/j.ijhydene.2018.05.110.
- [2] J. Li, G. Li, The utilization of renewable energy and the economic potential of offshore wind power supported by digital finance. Heliyon, 10(16), 2024. https://doi.org/10.1016/j.heliyon.2024.e35175.
- [3] Al Hadi, C.A.S. Silva, E. Hossain, R. Challoo, Algorithm for demand response to maximize the penetration of renewable energy, IEEE Access 8, 55279-55288, 2020. https://doi.org/10.1109/ACCESS .2020.2981877.
- [4] M. Ebeed, S. Ali, A.M. Kassem, M. Hashem, S. Kamel, A.G. Hussien, F. Jurado, E.A Mohamed, Solving stochastic optimal reactive power dispatch using an Adaptive Beluga Whale optimization considering uncertainties of renewable energy resources and the load growth. Ain Shams Engineering Journal, 102762, 2024. https://doi.org/10.1016/j.asej.2024.102762.
- [5] S.A. Mansouri, A. Ahmarinejad, M. Ansarian, M.S. Javadi, J.P.S. Catalao, Stochastic planning and operation of energy hubs considering demand response programs using Benders decomposition approach.

- International Journal of Electrical Power Energy Systems, 120, 106030, 2020. https://doi.org/10.1016/j.ijepes.2020.106030.
- [6] R. Kaluthanthrige, A.D. Rajapakse, Demand response integrated day-ahead energy management strategy for remote off-grid hybrid renewable energy systems. International Journal of Electrical Power Energy Systems, 129, 106731, 2021. https://doi.org/10.1016/ j.ijepes.2020.106731.
- [7] S.S Gul, D. Suchitra, A multistage coupon incentive-based demand response in energy market. Ain Shams Engineering Journal, 15(3), 102468, 2024. https://doi.org/10.1016/j.asej.2023.102468.
- [8] S. Nojavan, M.T. Hagh, K. Taghizad-Tavana, M. Ghanbari-Ghalehjoughi, Optimal demand response aggregation in wholesale electricity markets: Comparative analysis of polyhedral; ellipsoidal and box methods for modeling uncertainties. Heliyon 10(10), 2024. https://doi.org/10.1016/j.heliyon.2024.e31523.
- [9] L. Liu, H. Matayoshi, M. E. Lotfy, M. Datta, T. Senjyu, Load frequency control using demand response and storage battery by considering renewable energy sources. Energies, 11(12), 3412, 2018. https://doi. org/10.3390/en11123412
- [10] A. S. Roberts, L. Meegahapola, A. Vahidnia, Frequency Control using Dynamic Demand Response and Grid-Scale Battery Energy Storage Systems: An Australian Case Study. In 2024 IEEE 34th Australasian Universities Power Engineering Conference (AUPEC) (pp. 1-6). IEEE, 2024. https://doi.org/10.1109/AUPEC 62273.2024.10807590
- [11] M. Hu, F. Xiao, Price-responsive model-based optimal demand response control of inverter air conditioners using genetic algorithm. Applied Energy, 219, 151-164, 2018. https://doi.org/10.1016/j.apenergy.2018.03.036.
- [12] M. Afzalan, F. Jazizadeh, Residential loads flexibility potential for demand response using energy consumption patterns and user segments. Applied Energy, 254, 113693, 2019. https://doi.org/10.1016/j.apenergy.2019.113693.
- [13] H. Golmohamadi, R. Keypour, B. Bak-Jensen, J.R. Pillai, A multi-agent based optimization of residential and industrial demand response aggregators. International Journal of Electrical Power Energy Systems, 107, 472-485, 2019. https://doi.org/10.1016/j.ijepes.2018.12.020.
- [14] S. Liu, P.X. Liu, X. Wang, Stability analysis and compensation of network-induced delays in communication-based power system control: A survey. ISA Transactions, 66, 143-153, 2017. https://doi.org/10.1016/j.isatra.2016.09.022.
- [15] D. Katipoğlu, Ş. Sönmez, S. Ayasun, A. Naveed, The effect of demand response control on stability delay margins of load frequency control systems with communication time-delays. The Turkish Journal of Electrical Engineering Computer Sciences, 29(3),

- 1383-1400, 2021. https://doi.org/10.3906/elk-2006-165.
- [16] D. Katipoğlu, Ş. Sönmez, S. Ayasun, A. Naveed, Impact of participation ratios on the stability delay margins computed by direct method for multiple-area load frequency control systems with demand response. Automatika, 63(1), 185-197, 2022. https://doi.org/10. 1080/00051144.2021.2020554.
- [17] S. Saxena, Y.V. Hote, Decentralized PID load frequency control for perturbed multi-area power systems. International Journal of Electrical Power & Energy Systems, 81, 405-415, 2016. https://doi.org/10.1016/j.ijepes.2016.02.041.
- [18] V.P. Singh, P. Samuel, N. Kishor, Impact of demand response for frequency regulation in two-area thermal power system. International Transactions on Electrical Energy Systems, 27(2), e2246, 2017. https://doi.org/10.1002/etep.2246.
- [19] X. Wang, X. Zhang, H. Sun, Real-time incentive design under unknown demand response curves via a proportional-integral control framework, IEEE Tran. Smart Grid 14(5) (2023) 3654-3667, https://doi.org/10.1109/TSG.2023.3245672.
- [20] V. Çelik, M.T. Özdemir, G. Bayrak, The effects on stability region of the fractional-order PI controller for one-area time-delayed load-frequency control systems. Transactions of the Institute of Measurement and Control, 39(10), 1509-1521, 2017. https://doi.org/10 .1177/0142331216642839.
- [21] V. Çelik, M.T. Özdemir, K.Y. Lee, Effects of fractional-order PI controller on delay margin in singlearea delayed load frequency control systems. Journal of Modern Power Systems and Clean Energy, 7(2), 380-389, 2019. https://doi.org/10.1007/s40565-018-0458-5.
- [22] B. Yildirim, M. Gheisarnejad, M.H. Khooban, A robust non-integer controller design for load frequency control in modern marine power grids. IEEE Transactions on Emerging Topics in Computational Intelligence, 6(4), 852-862, 2021. https://doi.org/10.1109/TETCI.2021 .3114735.
- [23] A. Tabak, Fractional order frequency proportional-integral-derivative control of microgrid consisting of renewable energy sources based on multi-objective grasshopper optimization algorithm. Transactions of the Institute of Measurement and Control, 44(2), 378-392, 2022. https://doi.org/10.1177/01423312211034660.
- [24] F. Asadi, N. Abut, Kharitonov's theorem: A good starting point for robust control. The International Journal of Electrical Engineering & Education, 58(1), 57-82, 2021. https://doi.org/10.1177/0020720919829 708.
- [25] M. Ebrahimi, E. S. Alaviyan Shahri, A. Alfi, A graphical method-based Kharitonov theorem for robust stability analysis of incommensurate fractional-order uncertain systems. Computational and Applied Mathematics, 43(2), 101, 2024. https://doi.org/ 10.1007/s40314-024-02610-z

- [26] S.K. Pandey, J. Dey, S. Banerjee, Modified Kharitonov theorem based optimal PID controller design for MIMO systems. Journal of Electrical Engineering & Technology, 18(3), 2317-2334, 2023. https://doi .org/10.1007/s42835-022-01329-3
- [27] N. Tan, I. Kaya, C. Yeroglu, D.P. Atherton, Computation of stabilizing PI and PID controllers using the stability boundary locus. Energy Conversion and Management, 47(18-19), 3045-3058, 2006. https://doi.org/10.1016/j.enconman.2006.03.022.
- [28] M.T. Söylemez, N. Munro, H. Baki, Fast calculation of stabilizing PID controllers. Automatica, 39(1), 121-126, 2003. https://doi.org/10.1016/S0005-1098(02)00180-2
- [29] O. Turksoy, S. Ayasun, Y. Hames, Ş. Sönmez, Computation of robust PI-based pitch controller parameters for large wind turbines. IEEE Canadian Journal of Electrical and Computer Engineering, 43(1), 57-63, 2019. https://doi.org/10.1109/CJECE.2019. 2923050.
- [30] Ş. Sönmez, S. Ayasun, Computation of PI controllers ensuring desired gain and phase margins for two-area load frequency control system with communication time delays. Electric Power Components and Systems, 46(8), 938-947, 2018. https://doi.org/10.1080/1532 5008.2018.1509914.
- [31] H. Gündüz, Ş. Sonmez, S. Ayasun, A comprehensive gain and phase margins-based stability analysis of micro-grid frequency control system with constant communication time delays. IET Generation, Transmission Distribution, 11(3), 719-729, 2017. https://doi.org/10.1049/iet-gtd.2016.0644.
- [32] M.T. Özdemir, The effects of the FOPI controller and time delay on stability region of the fuel cell microgrid. International Journal of Hydrogen Energy, 45(60), 35064-35072, 2020. https://doi.org/10.1016/j.ijhydene. 2020.05.211.
- [33] H. Gündüz, Ş. Sönmez, S. Ayasun, Identification of gain and phase margins based robust stability regions for a time-delayed micro-grid system including fractional-order controller in presence of renewable power generation. The Turkish Journal of Electrical Engineering Computer Sciences, 30(3), 1097-1114, 2022. https://doi.org/10.55730/1300-0632.3829.
- [34] S. Sondhi, Y.V. Hote, Fractional order PID controller for perturbed load frequency control using Kharitonov's theorem. International Journal of Electrical Power Energy Systems, 78, 884-896, 2016. https://doi.org/10.1016/j.ijepes.2015.11.103.
- [35] R. Lamba, S.K. Singla, S. Sondhi, Design of fractional order PID controller for load frequency control in perturbed two area interconnected system. Electric Power Components and Systems, 47(11-12), 998-1011, 2016. https://doi.org/10.1080/15325008.2019.16607 36.

- [36] C.H. Chang, K.W. Han, Gain margins and phase margins for control systems with adjustable parameters. Journal of Guidance, Control, and Dynamics, 13(3), 404–408, 1990. https://doi.org/10.2514/3.25351.
- [37] Z.Y. Nie, Q.G. Wang, M. Wu, Y. He, Combined gain and phase margins. ISA Transactions, 48(4), 428-433, 2009. https://doi.org/10.1016/j.isatra.2009.07.004.
- [38] Simulink, Simulation and model-based design, Natick, MA, USA: MathWorks, 2019.
- [39] S.A. Pourmousavi, M.H. Nehrir, Introducing dynamic demand response in the LFC model. IEEE Transactions on Power Systems, 29(4), 1562-1572, 2014. https://doi.org/10.1109/TPWRS.2013.2296696.
- [40] J. Sharma, Y.V. Hote, R. Prasad, PID controller design for interval load frequency control system with communication time delay. Control Engineering Practice, 89, 154-168, 2019. https://doi.org/10.1016/j.conengprac.2019.05.016.
- [41] A.J. Samy Jeya Veronica, N. Senthil Kumar, F. Gonzalez-Longatt, Robust PI controller design for frequency stabilisation in a hybrid microgrid system considering parameter uncertainties and communication time delay. IET Generation, Transmission Distribution, 13(14), 3048-3056, 2019. https://doi.org/10.1049/iet-gtd.2018.5240.
- [42] F.A. Hasan, A.T. Humod, L.J. Rashad, Robust decoupled controller of induction motor by combining PSO and Kharitonov's theorem. Engineering Science and Technology, an International Journal, 23(6), 1415-1424, 2020. https://doi.org/10.1016/j.jestch.2020.04.004.
- [43] K.S. Ko, D.K. Sung, The effect of EV aggregators with time-varying delays on the stability of a load frequency control system. IEEE Transactions on Power Systems, 33(1), 669-680, 2017. https://doi.org/10.1109/TPWRS. 2017.2690915.
- [44] D. Katipoğlu, Stability analysis using fractional-order PI controller in a time-delayed single-area load frequency control system with demand response. Advances in Electrical Computer Engineering, 23(2), 2023. https://doi.org/10.4316/AECE.2023.02005
- [45] D. Katipoğlu, Ş. Sönmez, S. Ayasun, Dinamik talep cevabı içeren zaman gecikmeli iki bölgeli yük frekans kontrol sistemlerinin kararlılık bölgelerinin hesaplanması. Gazi Üniversitesi Mühendislik Mimarlık Fakültesi Dergisi, 39(1), 431-442, 2024. https://doi.org/10.17341/gazimmfd.951415
- [46] D. Katipoğlu, S. Soylu, Design of optimal FOPI controller for two-area time-delayed load frequency control system with demand response. Journal of Electrical Engineering & Technology, 19(7), 4073-4085, 2024. https://doi.org/10.1007/s42835-024-01900-0

